Progress In Electromagnetics Research, *PIER 31, 31–54, 2001*

THEORETICAL MODELING OF MULTI-SLEEVE MONOPOLE ANTENNAS

Z. Shen

School of Electrical and Electronic Engineering
Nanyang Technological University
Nanyang Avenue, Singapore 639798

R. H. MacPhie

Department of Electrical and Computer Engineering
University of Waterloo
Waterloo, Ontario, Canada N2L 3G1

Abstract–This article presents a numerical technique based on the modal-expansion method for modeling a multi-sleeve monopole antenna fed through an infinite ground-plane by a coaxial transmission line. The modal-expansion analysis is facilitated by introducing a perfectly conducting boundary at a variable height over the ground-plane of the monopole. The resulting structure is then divided into a number of regions and the electromagnetic field components in each region are expanded into the summation of its modal functions. The current distribution over the monopole and sleeve surfaces as well as the antenna's input impedance are computed by finding the expansion coefficients through matching the tangential field components across the regional interfaces. Numerical results for the surface current distribution and input impedance are presented and discussed with emphasis laid on single- and double-sleeve monopole antennas.

1. INTRODUCTION

Monopole antennas have been widely used in airborne and ground-based communication systems. Monopole antennas on portable telephones can be observed in daily life. A monopole with an infinite ground-plane has the very similar radiation characteristics in the half-space over the ground-plane as a dipole according to the method of images. A considerable amount of theoretical and experimental work has been devoted to the problem of a conventional monopole [1, 2]. The sleeve-monopole antenna is a modification of the conventional monopole antenna with the outer conductor of the coaxial feed line projected over the ground plane. The interesting and desirable property of the sleeve monopole is its broad-band characteristic [3, 4].

In spite of the fact that the sleeve monopole exhibits broader bandwidth over conventional monopole antennas, it was not thoroughly and intensively investigated in the past. Taylor [3] and King [1] employed the method of images and the superposition theorem to determine the surface currents on the monopole and on the sleeve, but they did not take into account the effect of the different radii of the monopole and the sleeve. Therefore, it would be difficult to generalize their technique to multi-sleeve monopoles. Taylor [3] also carried out careful measurements of the current distribution and input impedance of a single sleeve monopole. Rispin and Chang [5] introduced a simple thin-wire analysis for sleeve antennas as well as other wire antennas by constructing the standing wave current on the antenna surface. Wunsch [6] determined the impedance and radiation pattern of the sleeve-monopole antenna by using a Fourier series representation of its surface current. A rigorous modal-expansion method for conventional monopole and sleeve-monopole antennas was recently developed by Shen and MacPhie [7, 8].

Experimental investigation of double- and multi-sleeve antennas indicated that a much wider bandwidth can be achieved by properly choosing the geometrical parameters. But to the authors' knowledge, no sound theoretical investigation has appeared. This article presents a theoretical analysis of a multi-sleeve monopole antenna by using the modal-expansion method [7, 8]. Our emphasis is laid on numerically examining the effect of the structural parameters on the input impedance and the current distribution on the monopole and the sleeves of single- and double-sleeve monopole antennas.

This article is organized as follows. Section 2 details the mathemati-

cal formulation for the multi-sleeve monopole problem. By introducing a perfectly conducting boundary parallel to the ground-plane over the monopole antenna, we are able to employ the modal-expansion method to rigorously analyze the antenna problem and accurately characterize the effects of the feed line and different radii of the monopole and the sleeves. Unlike using the perfectly matched boundary (PMB) in [8], where two problems with either electric or magnetic wall need to be solved, in this work we only employ the perfectly conducting boundary to reduce the computational effort by half. To make the technique even more efficient, we also introduce a circular disk to the top plate to greatly reduce the size of the matrices to be inverted. This is achieved without compromising the accuracy since the radiation is null in the vertical direction and the distance between the assumed plate and the ground plane is maintained to be several wavelengths for convergent results.

After assuming the conducting boundary, we divide the resulting structure into a number of subregions. Starting with the Maxwell's equation, we then derive the modal functions for every subregion and expand the electromagnetic fields in all the subregions by the summation of their modal functions. By matching the tangential electric and magnetic components along the regional interfaces, we can find the expansion coefficients from which the surface current distribution, input impedance, and radiation pattern result. Section 3 gives numerical results for single- and double-sleeve monopole antennas. Current distributions, input impedances, and radiation patterns are numerically examined for different values of the geometrical parameters. Conclusions and our contributions are summarized in Section 4.

2. FORMULATION

The theoretical model we employ to characterize an N-sleeve monopole antenna fed by a coaxial transmission line is shown in Fig. 1, where a perfectly conducting boundary is placed parallel to the ground plane at a distance d_0 above the monopole. Since the radiation is null in the vertical direction, it is feasible to introduce a disk on the conducting plate to greatly reduce the size of the matrices to be inverted, which makes this technique very efficient. The computational efficiency is gained without compromising the accuracy since the separation between the introduced plate and the ground-plane can be a few wavelengths so that good convergent results can be obtained [8]. It will be

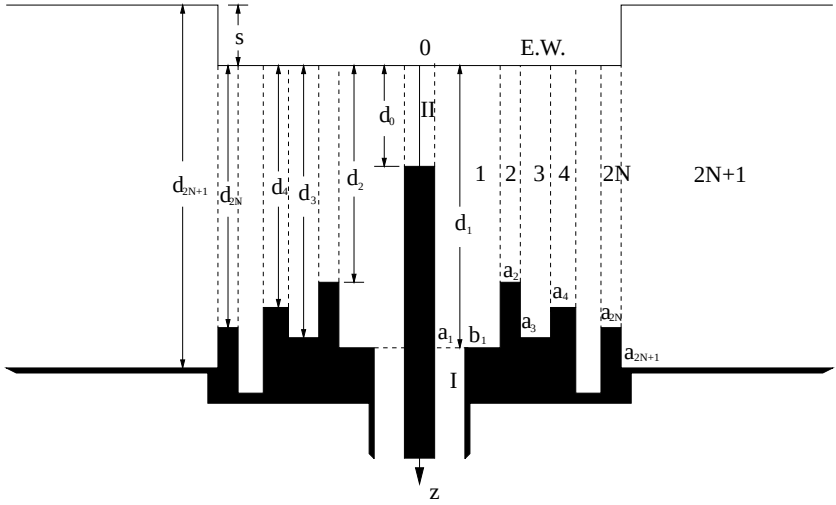

Figure 1. Analysis model of a multi-sleeve monopole antenna.

seen later that the presence of the conducting plate and the loading disk does not have significant influence on antenna's characterization.

As indicated in Fig. 1, the inner and outer radii of the coaxial feed line are a_1 and b_1, respectively. The interior and exterior radii of the i-th sleeve are, respectively, a_{2i} and a_{2i+1} for $i = 1, 2, \ldots, N$. The separation distances from the top disk to the grooves and sleeves are d_{2i-1} and d_{2i} $(i = 1, 2, \ldots, N)$. The distance between the ground-plane and the postulated wall is d_{2N+1}. As described in [8], after introducing the conducting boundary on the top of the antenna, the resulting structure of this N-sleeve monopole can be analyzed by the modal-expansion method.

As illustrated in Fig. 1, the whole structure of interest is first divided into $(2N + 3)$ subregions: $\mathrm{I}, \mathrm{II}, 1, 2, \ldots, 2N$ and $2N + 1$. Since the structure and the incident dominant TEM mode in the coaxial feed waveguide are axis-symmetric (no ϕ variation), only three field components (E_z, E_ρ, and H_ϕ) are non-zero.

Starting with Maxwell's curl equations

$$\nabla \times \vec{H} = j\omega\epsilon\vec{E} \tag{1a}$$

$$\nabla \times \vec{E} = -j\omega\mu\vec{H} \tag{1b}$$

and using the relation $\frac{\partial}{\partial\phi} = 0$, one can derive the following expressions

for three non-zero field components E_z, E_ρ, and H_ϕ.

$$E_\rho = \frac{-1}{j\omega\epsilon}\frac{\partial}{\partial z}H_\phi \tag{2a}$$

$$E_z = \frac{1}{j\omega\epsilon}\frac{1}{\rho}\frac{\partial}{\partial \rho}(\rho H_\phi) \tag{2b}$$

$$\frac{\partial^2 H_\phi}{\partial \rho^2} + \frac{1}{\rho}\frac{\partial H_\phi}{\partial \rho} + \frac{\partial^2 H_\phi}{\partial z^2} + \left(k^2 - \frac{1}{\rho^2}\right) H_\phi = 0 \tag{2c}$$

where $k = \omega\sqrt{\mu\epsilon}$ is the wave number. It is noted that the $\exp(j\omega t)$ time dependence is assumed and suppressed for all the fields throughout this article. Based on these relations, one has no difficulty in finding the field expressions for all the subregions in Fig. 1; they are summarized in the following.

For the coaxial feed waveguide (Region I), the transverse electromagnetic fields with respect to the z-axis can be represented by

$$E_\rho^I = \sum_{n=0}^{N_I} \left(A_{In}\exp[j\beta_{In}(z-d_1)] + A_{Rn}\exp[-j\beta_{In}(z-d_1)]\right) e_{In\rho} \tag{3a}$$

$$H_\phi^I = \sum_{n=0}^{N_I} (-A_{In}\exp[j\beta_{In}(z-d_1)] + A_{Rn}\exp[-j\beta_{In}(z-d_0)]) Y_{In} e_{In\rho} \tag{3b}$$

where $\mathbf{A}_{In} = (A_{I0}, A_{I1}, \ldots, A_{IN_I})^T$ and $\mathbf{A}_{Rn} = (A_{R0}, A_{R1}, \ldots, A_{RN_I})^T$ with T representing the transpose operation, are the incident and reflected modal amplitude column vectors in the coaxial feed waveguide; $\beta_{In} = \sqrt{k_0^2\epsilon_r^I - (x_{In}/a_1)^2}$ is the propagation constant with x_{In}/a_1 being the cutoff wavenumber of the n-th mode, and $Y_{In} = \frac{\omega\epsilon_I}{\beta_{In}}$ is the modal admittance. The normalized transverse modal electric field $e_{In\rho}$ has the form of [9]

$$e_{In\rho} = \begin{bmatrix} \dfrac{1}{\sqrt{2\pi\ln(b_1/a_1)}}\dfrac{1}{\rho}, & \text{for } n = 0 \\ N_{In}\dfrac{x_{In}}{a_1}Z_0'\left(\dfrac{x_{In}}{a_1}\rho\right), & \text{for } n > 0 \end{bmatrix} \tag{4}$$

where

$$Z_0\left(\frac{x_{In}}{a_1}\rho\right) = J_0\left(\frac{x_{In}}{a_1}\rho\right) Y_0(x_{In}) - Y_0\left(\frac{x_{In}}{a_1}\rho\right) J_0(x_{In})$$

$$N_{In} = \frac{\sqrt{\pi}}{2}\frac{1}{\sqrt{\left[Y_0(x_{In})/Y_0\left(\dfrac{b_1 x_{In}}{a_1}\right)\right]^2 + 1}}$$

and J_0 and Y_0 are the first and second kind of Bessel functions of order 0, respectively, Z_0' in (4) denotes the derivative of Z_0 with respect to its entire argument. It is noted that the cutoff wavenumber x_{In}/a_1 is the solution to the equation $Z_0\left(\frac{x_{In}}{a_1}b_1\right)=0$.

In Region II we have

$$E_z^{II} = \frac{1}{j\omega\epsilon_0}\sum_{n=0}^{N_{II}} A_n^{II}\cos\frac{n\pi z}{d_0}\frac{J_0\left(\gamma_n^{II}\rho\right)}{J_0\left(\gamma_n^{II}a_1\right)} \tag{5a}$$

$$E_\rho^{II} = \sum_{n=1}^{N_{II}} \frac{n\pi A_n^{II}}{j\omega\epsilon_0 d_0}\sin\frac{n\pi z}{d_0}\frac{J_1\left(\gamma_n^{II}\rho\right)}{J_0\left(\gamma_n^{II}a_1\right)} \tag{5b}$$

$$H_\phi^{II} = \sum_{n=0}^{N_{II}} A_n^{II}\cos\frac{n\pi z}{d_0}\frac{J_1\left(\gamma_n^{II}\rho\right)}{\gamma_n^{II}J_0\left(\gamma_n^{II}a_1\right)} \tag{5c}$$

where $\left(\gamma_n^{II}\right)^2 = k_0^2-(n\pi/d_0)^2$, A_n^{II} is the expansion coefficient to be determined.

The expressions for the electromagnetic fields in Region 1 can be obtained by employing the resonator method [8, 10].

$$\begin{aligned} E_z^1 = {} & \frac{1}{j\omega\epsilon_0}\sum_{n=0}^{N_1}\left[U_{1n}(\rho)A_{1n}+V_{1n}(\rho)B_{1n}\right]\cos\frac{n\pi z}{d_1} \\ & -\sum_{n=0}^{N_1'} C_n e_{2nz}(\rho)\frac{\cosh(\alpha_n z)}{\alpha_n\sinh(\alpha_n d_1)} \end{aligned} \tag{6a}$$

$$\begin{aligned} E_\rho^1 = {} & \sum_{n=0}^{N_1}\frac{-n\pi}{j\omega\epsilon_0 d_1\gamma_{1n}^2}\left[U_{1n}'(\rho)A_{1n}+V_{1n}'(\rho)B_{1n}\right]\sin\frac{n\pi z}{d_1} \\ & +\sum_{n=0}^{N_1'} C_n e_{2n\rho}(\rho)\frac{\sinh(\alpha_n z)}{\sinh(\alpha_n d_1)} \end{aligned} \tag{6b}$$

$$\begin{aligned} H_\phi^1 = {} & \sum_{n=0}^{N_1}\frac{-1}{\gamma_{1n}^2}\left[U_{1n}'(\rho)A_{1n}+V_{1n}'(\rho)B_{1n}\right]\cos\frac{n\pi z}{d_1} \\ & -\sum_{n=0}^{N_1'} C_n e_{2n\rho}(\rho)\frac{j\omega\epsilon_0\cosh(\alpha_n z)}{\alpha_n\sinh(\alpha_n d_1)} \end{aligned} \tag{6c}$$

where $\gamma_{in}^2 = k_0^2 - \left(\frac{n\pi}{d_i}\right)^2$, and

$$U_{in}(\rho) = \frac{J_0(\gamma_{in}\rho)Y_0(\gamma_{in}a_i) - Y_0(\gamma_{in}\rho)J_0(\gamma_{in}a_i)}{J_0(\gamma_{in}a_{i+1})Y_0(\gamma_{in}a_i) - Y_0(\gamma_{in}a_{i+1})J_0(\gamma_{in}a_i)} \tag{7a}$$

$$V_{in}(\rho) = \frac{J_0(\gamma_{in}a_{i+1})Y_0(\gamma_{in}\rho) - Y_0(\gamma_{in}a_{i+1})J_0(\gamma_{in}\rho)}{J_0(\gamma_{in}a_{i+1})Y_0(\gamma_{in}a_i) - Y_0(\gamma_{in}a_{i+1})J_0(\gamma_{in}a_i)} \tag{7b}$$

for $i = 1, 2, \ldots, 2N$. In (6) $e_{2nz}(\rho)$ and $e_{2n\rho}(\rho)$ are the longitudinal and transverse electric field components in a coaxial waveguide whose inner and outer radii are a_1 and a_2, respectively; $\alpha_n^2 = (x_{1n}/a_1)^2 - k_0^2$ with x_{1n}/a_1 being the cutoff wavenumber of the n-th mode in that waveguide. Expression for $e_{2n\rho}(\rho)$ is the same as (4) for $e_{In\rho}(\rho)$ with x_{In} replaced by x_{1n} and b_1 with a_2.

The electromagnetic fields in Region i $(i = 2, 3, \ldots, 2N)$ are as follows:

$$E_z^i = \frac{1}{j\omega\epsilon_0}\sum_{n=0}^{N_i}\left[U_{in}(\rho)A_{in} + V_{in}(\rho)B_{in}\right]\cos\frac{n\pi z}{d_i} \tag{8a}$$

$$E_\rho^i = \sum_{n=0}^{N_i}\frac{-n\pi}{j\omega\epsilon_0 d_i\gamma_{in}^2}\left[U'_{in}(\rho)A_{in} + V'_{in}(\rho)B_{in}\right]\sin\frac{n\pi z}{d_i} \tag{8b}$$

$$H_\phi^i = \sum_{n=0}^{N_i}\frac{-1}{\gamma_{in}^2}\left[U'_{in}(\rho)A_{in} + V'_{in}(\rho)B_{in}\right]\cos\frac{n\pi z}{d_i} \tag{8c}$$

where $U_{in}(\rho)$ and $V_{in}(\rho)$ are defined in (7). Finally, the electromagnetic field components in Region $2N+1$ have the form of

$$E_z^{2N+1} = \frac{1}{j\omega\epsilon_0}\sum_{n=0}^{N_{2n+1}} A_{(2N+1)n}\cos\frac{n\pi(z+s)}{d_{2N+1}}\frac{H_0^{(2)}(\gamma_{(2N+1)n}\rho)}{H_0^{(2)}(\gamma_{(2N+1)n}a_{2N+1})} \tag{9a}$$

$$E_\rho^{2N+1} = \sum_{n=0}^{N_{2N+1}}\frac{n\pi A_{(2N+1)n}}{j\omega\epsilon_0 d_{2N+1}}\sin\frac{n\pi(z+s)}{d_{2N+1}}\frac{H_1^{(2)}(\gamma_{(2N+1)n}\rho)}{\gamma_{(2N+1)n}H_0^{(2)}(\gamma_{(2N+1)n}a_{2N+1})} \tag{9b}$$

$$H_\phi^{2N+1} = \sum_{n=0}^{N_{2N+1}} A_{(2N+1)n}\cos\frac{n\pi(z+s)}{d_{2N+1}}\frac{H_1^{(2)}(\gamma_{(2N+1)n}\rho)}{\gamma_{(2N+1)n}H_0^{(2)}(\gamma_{(2N+1)n}a_{2N+1})} \tag{9c}$$

where $\gamma_{(2N+1)n}^2 = k_0^2 - \left(\frac{n\pi}{d_{2N+1}}\right)^2$, and $H_0^{(2)}$ and $H_1^{(2)}$ are the outgoing second kind Hankel functions of order 0 and 1, respectively.

After having found all the field expressions, we are now at the position to match these field components along the regional interfaces. In order to efficiently handle this multi-sleeve structure, a recursive algorithm is desired. In the following, we shall deal with the field-matching process [8] for one groove cell first and derive the recursive matrix equations for the expansion coefficients and then use the derived recursive relation to treat the general multi-layered problem. Consider the groove between sleeve i and sleeve $i+1$, as shown in Fig. 2, which is scaled for a better view. The groove region is denoted as $2i+1$, while the regions of sleeves i and $i+1$ are, respectively, $2i$ and $2i+2$. The field expressions for the three regions are given in (8).

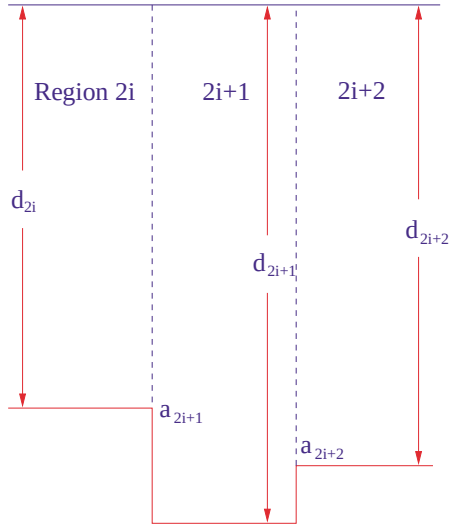

Figure 2. The i-th groove cell.

Application of the boundary conditions that the tangential electromagnetic fields must be continuous at the interface $\rho = a_{2i+1}$ between Regions $2i$ and $2i+1$ results in the following matrix equations:

$$\mathbf{B}_{2i+1} = \mathbf{F}_{A(i+1)} \mathbf{A}_{2i} \tag{10a}$$

$$\mathbf{D}_{C(2i)} \mathbf{A}_{2i} + \mathbf{D}_{D(2i)} \mathbf{B}_{2i} = \mathbf{F}^{T}_{A(i+1)} \left[\mathbf{D}_{A(2i+1)} \mathbf{A}_{2i+1} + \mathbf{D}_{B(2i+1)} \mathbf{B}_{2i+1} \right] \tag{10b}$$

where

$$F_{A(i+1)(n,m)} = \frac{\epsilon_n}{d_{2i+1}} \int_0^{d_{2i}} \cos \frac{n\pi z}{d_{2i+1}} \cos \frac{m\pi z}{d_{2i}} dz$$

$$D_{A(2i)} = \frac{-d_{2i}U'_{2i}(a_{2i})}{\epsilon_n \gamma^2_{(2i)n}}\delta_{nm}, \qquad D_{B(2i)} = \frac{-d_{2i}V'_{2i}(a_{2i})}{\epsilon_n \gamma^2_{(2i)n}}\delta_{nm}$$
$$D_{C(2i)} = \frac{-d_{2i}U'_{2i}(a_{2i+1})}{\epsilon_n \gamma^2_{(2i)n}}\delta_{nm}, \quad D_{D(2i)} = \frac{-d_{2i}V'_{2i}(a_{2i+1})}{\epsilon_n \gamma^2_{(2i)n}}\delta_{nm}$$

with $\epsilon_n = 1$ for $n = 0$, $\epsilon_n = 2$ for $n > 0$ and $\delta_{n,m} = 1$ for $n = m$, $\delta_{n,m} = 0$ for $n \neq m$. Similarly, enforcement of the boundary conditions that the tangential electromagnetic fields must be equal along the interface $\rho = a_{2i+2}$ between Regions $2i+1$ and $2i+2$ leads to

$$\mathbf{A}_{2i+1} = \mathbf{F}_{B(i+1)}\mathbf{B}_{2i+2} \tag{11a}$$
$$\mathbf{D}_{A(2i+2)}\mathbf{A}_{2i+2} + \mathbf{D}_{B(2i+2)}\mathbf{B}_{2i+2} = \mathbf{F}^T_{B(i+1)}\left[\mathbf{D}_{C(2i+1)}\mathbf{A}_{2i+1} + \mathbf{D}_{D(2i+1)}\mathbf{B}_{2i+1}\right] \tag{11b}$$

where

$$F_{B(i+1)(n,m)} = \frac{\epsilon_n}{d_{2i+1}}\int_0^{d_{2i+2}} \cos\frac{n\pi z}{d_{2i+1}}\cos\frac{m\pi z}{d_{2i+2}}dz.$$

From (10) and (11), one eliminates $\mathbf{A}_{2i+1}$ and $\mathbf{B}_{2i+1}$ and derives the relations between $\mathbf{A}_{2i}$, $\mathbf{B}_{2i}$, and $\mathbf{A}_{2i+2}$, $\mathbf{B}_{2i+2}$ as follows.

$$\mathbf{B}_{2i} = \mathbf{T}_{i,11}\mathbf{A}_{2i} + \mathbf{T}_{i,12}\mathbf{B}_{2i+2} \tag{12a}$$
$$\mathbf{A}_{2i+2} = \mathbf{T}_{i,21}\mathbf{A}_{2i} + \mathbf{T}_{i,22}\mathbf{B}_{2i+2} \tag{12b}$$

where

$$\mathbf{T}_{i,11} = \mathbf{D}^{-1}_{D(2i)}\left[\mathbf{F}^T_{A(i+1)}\mathbf{D}_{B(2i+1)}\mathbf{F}_{A(i+1)} - \mathbf{D}_{C(2i)}\right]$$
$$\mathbf{T}_{i,12} = \mathbf{D}^{-1}_{D(2i)}\mathbf{F}^T_{A(i+1)}\mathbf{D}_{A(2i+1)}\mathbf{F}_{B(i+1)}$$
$$\mathbf{T}_{i,21} = \mathbf{D}^{-1}_{A(2i+2)}\mathbf{F}^T_{B(i+1)}\mathbf{D}_{D(2i+1)}\mathbf{F}_{A(i+1)}$$
$$\mathbf{T}_{i,22} = \mathbf{D}^{-1}_{A(2i+2)}\left[\mathbf{F}^T_{B(i+1)}\mathbf{D}_{C(2i+1)}\mathbf{F}_{B(i+1)} - \mathbf{D}_{B(2i+2)}\right].$$

Equation (12) provides a recursive relation of the electromagnetic fields between two adjacent sleeve regions $2i$ and $2i+2$. It is noted that no matrix inversion is required for computing the transmission matrices in (12) since $\mathbf{D}_{D(2i)}$ and $\mathbf{D}_{D(2i)}$ are diagonal matrices. If the relation

$$\mathbf{B}_{2i+2} = \mathbf{\Gamma}_{2i+2}\mathbf{A}_{2i+2} \tag{13}$$

is known, one can easily obtain

$$\mathbf{B}_{2i} = \mathbf{\Gamma}_{2i}\mathbf{A}_{2i} \tag{14}$$

where

$$\mathbf{\Gamma}_{2i} = \mathbf{T}_{i,11} + \mathbf{T}_{i,12}\mathbf{\Gamma}_{2i+2}\left[\mathbf{I} - \mathbf{T}_{i,22}\mathbf{\Gamma}_{2i+2}\right]^{-1}\mathbf{T}_{i,21}$$

and $\mathbf{I}$ is the identity matrix.

Applying the boundary condition at the interface $\rho = a_{2N+1}$, we obtain

$$\mathbf{A}_{2N+1} = \mathbf{F}_{A(N+1)}\mathbf{A}_{2N} \tag{15a}$$

$$\mathbf{D}_{C(2N)}\mathbf{A}_{2N} + \mathbf{D}_{D(2N)}\mathbf{B}_{2N} = \mathbf{F}^{T}_{A(N+1)}\mathbf{Y}_{2N+1}\mathbf{A}_{2N+1}, \tag{15b}$$

which yields

$$\mathbf{B}_{2N} = \mathbf{\Gamma}_{2N}\mathbf{A}_{2N} \tag{16}$$

where

$$\mathbf{\Gamma}_{2N} = \mathbf{D}^{-1}_{D(2N)}\left[\mathbf{F}^{T}_{A(N+1)}\mathbf{Y}_{2N+1}\mathbf{F}_{A(N+1)} - \mathbf{D}_{C(2N)}\right]$$

$$F_{A(N+1)(n,m)} = \frac{\epsilon_n}{d_{2N+1}}\int_0^{d_{2i}} \cos\frac{n\pi(z+s)}{d_{2N+1}}\cos\frac{m\pi z}{d_{2N}}dz$$

$$Y_{2N+1,(n,m)} = \frac{\epsilon_n H_1^{(2)}(\gamma_{(2N+1)n}a_{2N+1})}{\gamma_{(2N+1)n}d_{2N+1}H_0^{(2)}\left(\gamma_{(2N+1)n}a_{2N+1}\right)}\delta_{nm}.$$

Given (16), one is able to determine $\mathbf{\Gamma}_{2N-2}$ using (12)–(14) for $i = N-1$. Repeatedly using (12)–(14), one can then get the matrix $\mathbf{\Gamma}_2$ for the relation

$$\mathbf{B}_2 = \mathbf{\Gamma}_2\mathbf{A}_2. \tag{17}$$

Finally, application of the boundary conditions that the tangential electromagnetic field components must be continuous at the interfaces $\rho = a_1$, $\rho = a_2$, and $z = d_1$ leads to the following matrix equations [8]:

$$\mathbf{B}_1 = \mathbf{F}_{A1}\mathbf{A}^{II} \tag{18a}$$

$$\mathbf{D}_{II}\mathbf{A}^{II} = \mathbf{F}^{T}_{A1}(\mathbf{D}_{A1}\mathbf{A}_1 + \mathbf{D}_{B1}\mathbf{B}_1) + \mathbf{W}_{II}\mathbf{C} \tag{18b}$$

$$\mathbf{A}_1 = \mathbf{F}_{B1}\mathbf{B}_2 \tag{19a}$$

$$\mathbf{D}_{A2}\mathbf{A}_2 + \mathbf{D}_{B2}\mathbf{B}_2 = \mathbf{F}^{T}_{B1}(\mathbf{D}_{C1}\mathbf{A}_1 + \mathbf{D}_{D1}\mathbf{B}_1) + \mathbf{W}_C\mathbf{C} \tag{19b}$$

$$\mathbf{C} = \mathbf{M}(\mathbf{A}_I + \mathbf{A}_R) \tag{20a}$$

$$\mathbf{Y}_I(\mathbf{A}_I - \mathbf{A}_R) = \mathbf{M}_A\mathbf{A}_1 + \mathbf{M}_B\mathbf{B}_1 + \mathbf{M}^T\mathbf{Y}_1\mathbf{C} \tag{20b}$$

where

$$D_{II,(n,m)} = \frac{d_0 J_1(\gamma_n^{II} a_1)}{\epsilon_n \gamma_n^{II} J_0(\gamma_n^{II} a_1)} \delta_{nm}, \qquad Y_{1,(n,m)} = \frac{-j\omega\epsilon_0}{\alpha_n \tanh(\alpha_n d_1)} \delta_{nm}$$

$$W_{II,(n,m)} = -\frac{j\omega\epsilon_0}{\alpha_m} e_{2m\rho}(a_1) \int_0^{d_0} \cos\frac{n\pi z}{d_0} \frac{\cosh(\alpha_m z)}{\sinh(\alpha_m d_1)} dz$$

$$W_{C,(n,m)} = -\frac{j\omega\epsilon_0}{\alpha_m} e_{2m\rho}(a_2) \int_0^{d_2} \cos\frac{n\pi z}{d_2} \frac{\cosh(\alpha_m z)}{\sinh(\alpha_m d_1)} dz$$

$$M_{n,m} = 2\pi \int_{a_1}^{b_1} e_{2n\rho}(\rho) e_{1m\rho}(\rho) \rho d\rho$$

$$M_{A,(n,m)} = 2\pi(-1)^m \int_{a_1}^{b_1} \frac{U'_{1m}(\rho)}{-\gamma_{1m}^2} e_{1n\rho}(\rho) \rho d\rho$$

$$M_{B,(n,m)} = 2\pi(-1)^m \int_{a_1}^{b_1} \frac{V'_{1m}(\rho)}{-\gamma_{1m}^2} e_{1n\rho}(\rho) \rho d\rho.$$

All the above integrals can be worked out in closed-form [11].

Using (17) and after some manipulations one has no difficulty in arriving at

$$\mathbf{A}_R = \left[2(\mathbf{I} - \mathbf{Y}_I^{-1}\mathbf{Y}_{L0})^{-1} - \mathbf{I}\right] \mathbf{A}_I \tag{21}$$

$$\mathbf{A}_{II} = \mathbf{Y}_M^{-1}\mathbf{W}_{II}\mathbf{M}(\mathbf{A}_I + \mathbf{A}_R) \tag{22}$$

$$\mathbf{A}_2 = \mathbf{Q}\left[\mathbf{F}_{B1}^T \mathbf{D}_{D1} \mathbf{F}_{A1} \mathbf{A}_{II} + \mathbf{W}_C \mathbf{M}(\mathbf{A}_I + \mathbf{A}_R)\right] \tag{23}$$

where

$$\mathbf{Y}_{L0} = \left[\left(\mathbf{M}_A \mathbf{F}_{B1} \mathbf{\Gamma}_2 \mathbf{Q} \mathbf{F}_{B1}^T \mathbf{D}_{D1} \mathbf{F}_{A1} + \mathbf{M}_B \mathbf{F}_{A1}\right) \mathbf{Y}_M^{-1} \mathbf{W}_{II} + \mathbf{M}^T \mathbf{Y}_1\right] \mathbf{M}$$

$$\mathbf{Y}_M = \mathbf{D}_{II} - \mathbf{F}_{A1}^T \mathbf{D}_{B1} \mathbf{F}_{A1} - \mathbf{F}_{A1}^T \mathbf{D}_{A1} \mathbf{F}_{B1} \mathbf{\Gamma}_2 \mathbf{Q} \mathbf{F}_{B1}^T \mathbf{D}_{D1} \mathbf{F}_{A1}$$

with $\mathbf{Q} = \left[\mathbf{D}_{A2} + \mathbf{D}_{B2}\mathbf{\Gamma}_2 - \mathbf{F}_{B1}^T \mathbf{D}_{C1} \mathbf{F}_{B1} \mathbf{\Gamma}_2\right]^{-1}$. From (21) we can obtain the reflection coefficients for all of the modes in the coaxial feed waveguide assuming the incident column vector $\mathbf{A}_I$ is known (for example, $(1, 0, \ldots, 0)^T$). Other expansion coefficients can then be found from (10)–(12), (15) and (17)–(20). The input impedance of the multi-sleeve monopole antenna and the current distribution along the monopole and the sleeves can be straightforwardly calculated by using the computed expansion coefficients [8]. Based on the current distribution and employing the method of images [12, 13], we can then

calculate the far-zone radiation pattern. For the detailed formulation, the reader is referred to [8].

3. NUMERICAL EXAMPLES

Based on the formulation described in the previous section, a Fortran program was written for analyzing a monopole antenna with arbitrary number of sleeves. The validity of the formulation for conventional monopole [7] and single-sleeve monopole [8] was extensively verified. The formulation for the multi-sleeve case has been verified for its special single-sleeve case with different radii of the sleeve and checked by the power conservation consideration. The number of modes considered in each region follow the well-known criterion [14] and was numerically studied in [8]. The choice of $N_I = 2$ and $N_{II} = 80$ is adopted in all the computations reported in this article, and the relations

$$N_1' = \frac{a_2 - a_1}{b_1 - a_1} N_I \tag{24}$$

and

$$\frac{N_i}{d_i} = \frac{N_{II}}{d_0} \; for \; i = 1, 2, \ldots, 2N + 1 \tag{25}$$

are always respected for convergent results.

The influence of the postulated boundary on the calculation of the antenna's input impedance is examined with satisfactory convergence for all the cases considered. Figure 3 shows the convergence behavior of a single-sleeve monopole's input impedance with respect to the distances d_0 and s. It is seen that the impedance variation is negligible when $d_0 > 1.5\lambda$ and $s > 0.5\lambda$. For larger s, the impedance converges for smaller d_0. It should be mentioned that the existence of the metallic disk on the introduced conducting wall can make all the matrices to be inverted relatively small since the size of the matrices to be inverted is closely related to d_0 and has nothing to do with the separation $d_3 = d_2 + l + s$. Therefore, choosing a suitable s and using a small d_0 can make the modal-expansion analysis very efficient. Similar examination is carried out for a double-sleeve monopole antenna and the convergence behavior is illustrated in Figure 4 for distances d_0 and s. We can see that the results are quite good when $d_0 > 1.4\lambda$ and $s > 0.5\lambda$. The choices of $d_0 = 1.5\lambda$ and $s = 0.5\lambda$ are adopted in the later computations and will not be specifically stated in the examples considered.

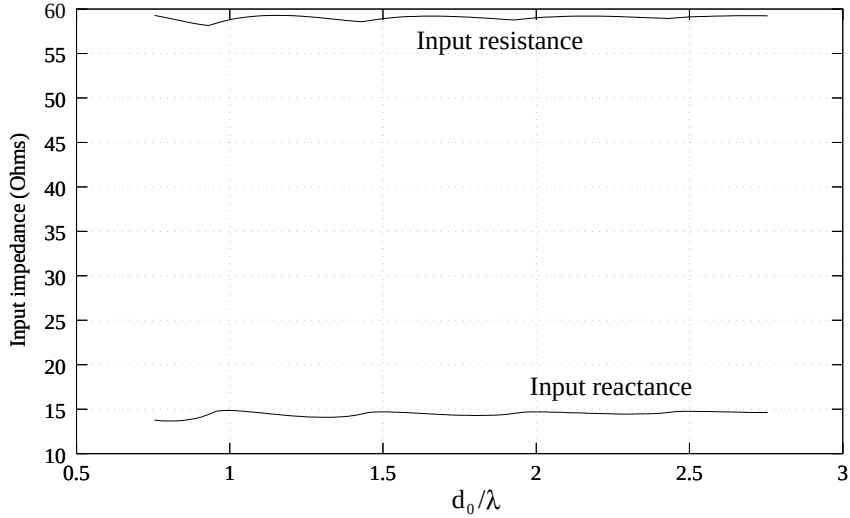

(a) $s = 0.8\lambda$

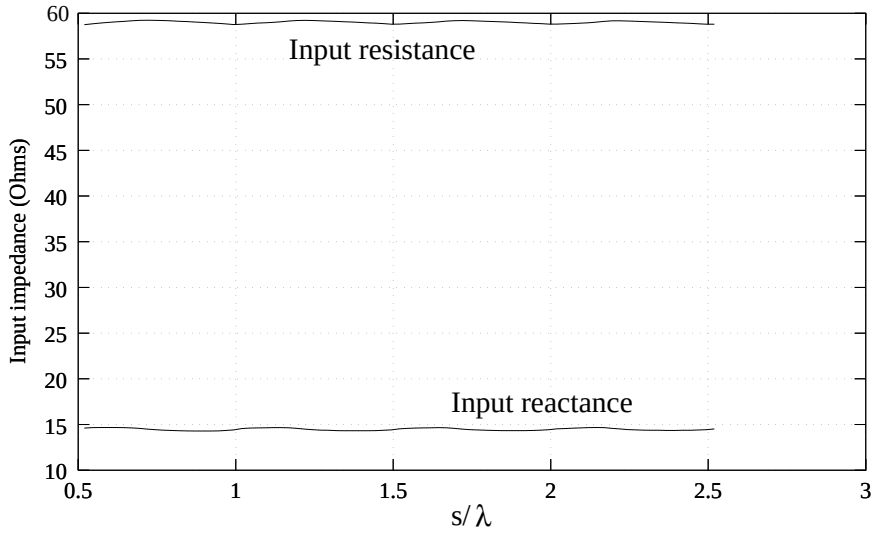

(b) $d_0 = 1.75\lambda$

Figure 3. Convergence behavior of the input impedance of a single-sleeve monopole antenna with respect to distances d_0 and s ($a_1 = 1.08\,\text{mm}$, $a_2 = b_1 = 3.5\,\text{mm}$, $\epsilon_{rI} = 2$, $a_3 = 4.5\,\text{mm}$, $d_2 = d_1 = d_0 + 32\,\text{mm}$, $d_3 = d_2 + 7.5\,\text{mm} + s$, $f = 2\,\text{GHz}$).

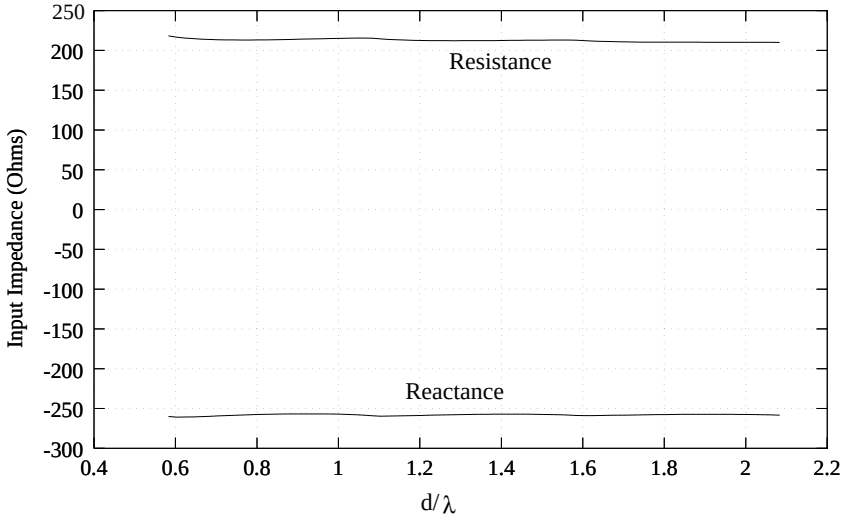

(a) $s = 0.5\lambda$

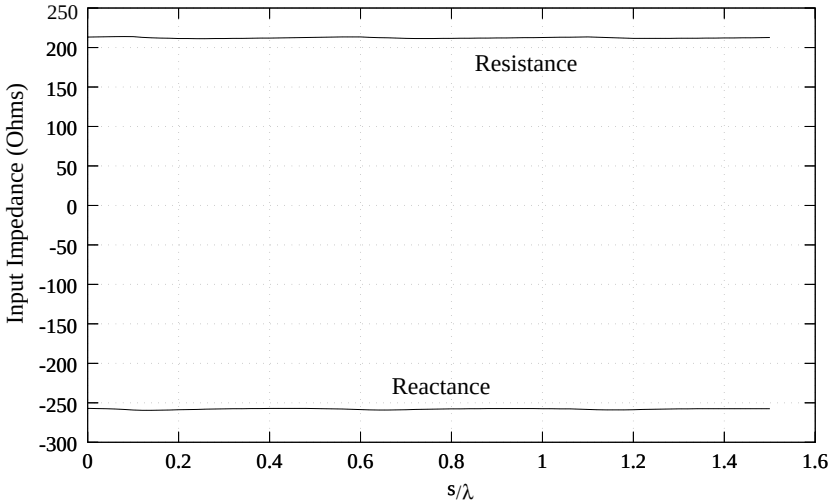

(b) $d_0 = 1.5\lambda$

Figure 4. Convergence behavior of the input impedance of a double-sleeve monopole antenna with respect to distances d_0 and s ($a_1 = 1.08\,\text{mm}$, $a_2 = b_1 = 3.5\,\text{mm}$, $\epsilon_{rI} = 2$, $a_3 = 3.75\,\text{mm}$, $a_4 = 4.5\,\text{mm}$, $a_5 = 4.75\,\text{mm}$, $d_1 = d_2 = d_0 + 30\,\text{mm}$, $d_3 = d_2 + 30\,\text{mm}$, $d_4 = d_2 + 12\,\text{mm}$, $d_5 = d_2 + 14\,\text{mm} + s$, $f = 1.9\,\text{GHz}$).

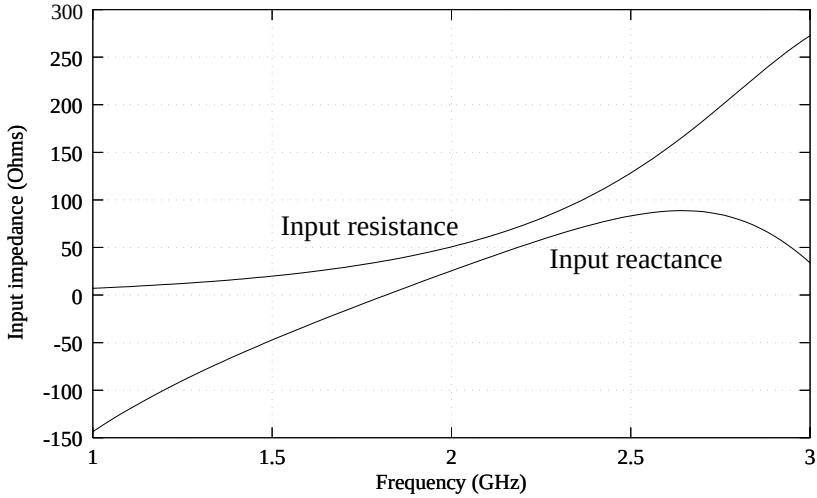

Figure 5. Input impedance of a conventional monopole ($a_1 = 1.08\,\text{mm},\ a_2 = b_1 = 3.5\,\text{mm},\ \epsilon_{rI} = 2,\ d_0 = 1.4\lambda,\ d_1 = d_0 + 37.5\,\text{mm} + s$).

Figures 5, 6, 7 gives a comparison of the input impedance of conventional monopole, single-sleeve monopole, and double-sleeve monopole antennas. For these three monopoles considered, the impedance's frequency characteristics are very similar because all of them have the first resonant frequency at 1.9 GHz. It should be pointed out that for sleeve monopoles, the input impedance is not only related to the total length of the antenna projected over the ground-plane, but also depends upon the length of the monopole and the length of the sleeve. Figures 8 and 9 presents the input impedance of single-sleeve and double-sleeve monopole antennas with different lengths of the monopole and sleeves. Both the input resistance and input reactance change dramatically for different compositions of monopole and sleeves even when the total length of the antenna (monopole + sleeves) is kept a constant. This is expected because the sleeves are part of the cylindrical radiator and different compositions of monopole and sleeves correspond to different locations of the feeding point, which should provide quite different impedance characteristics.

Figure 10 gives the return loss of the three monopole antennas considered in Figs. 5, 6, 7, respectively. It is interesting to note that the bandwidth of a single-sleeve monopole is wider than that of the conventional monopole. The $-10\,\text{dB}$ return loss bandwidth of the single-sleeve monopole is 22%, compared to 18% for the conven-

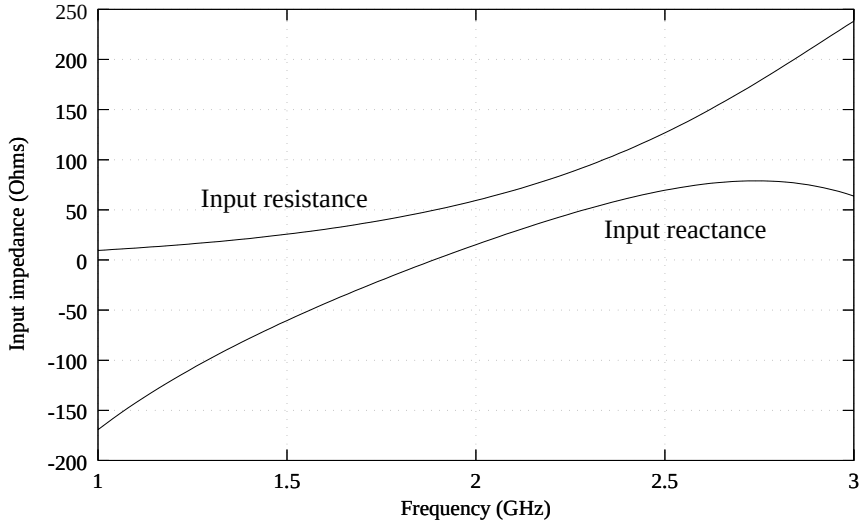

Figure 6. Input impedance of a single-sleeve monopole ($a_1 = 1.08\,\text{mm}$, $a_2 = b_1 = 3.5\,\text{mm}$, $\epsilon_{rI} = 2$, $a_3 = 4.5\,\text{mm}$, $d_2 = d_1 = d_0 + 32\,\text{mm}$, $d_3 = d_2 + 7.5\,\text{mm} + s$).

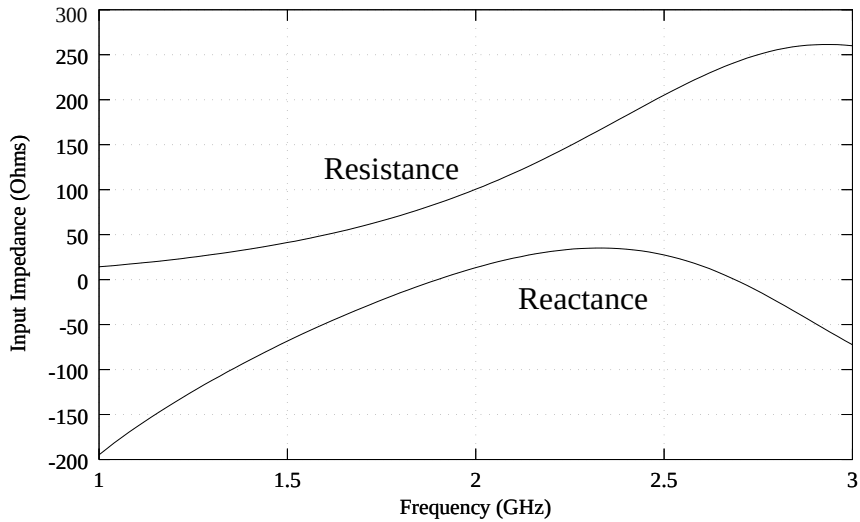

Figure 7. Input impedance of a double-sleeve monopole ($a_1 = 1\,\text{mm}$, $a_2 = b_1 = 4\,\text{mm}$, $\epsilon_{rI} = 1$, $a_3 = 4.25\,\text{mm}$, $a_4 = 5.25\,\text{mm}$, $a_5 = 5.5\,\text{mm}$, $d_1 = d_2 = d_0 + 27.5\,\text{mm}$, $d_3 = d_2 + 11.2\,\text{mm}$, $d_4 = d_2 + 4\,\text{mm}$, $d_5 = d_2 + 9\,\text{mm} + s$).

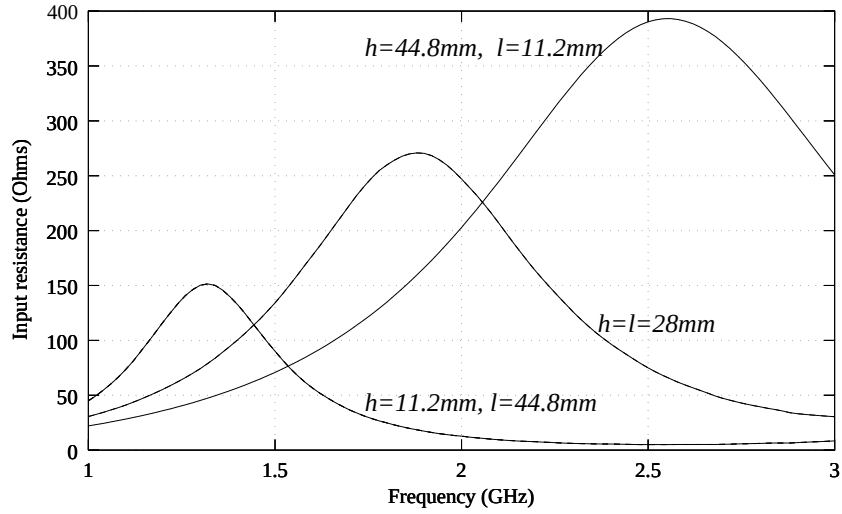

(a) Input resistance

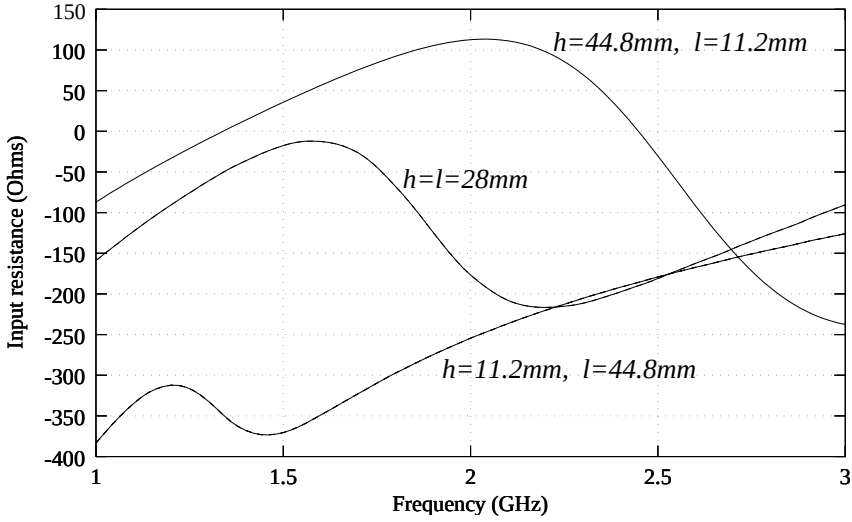

(b) Input reactance

Figure 8. Input impedance of single-sleeve monopole antennas with different monopole and sleeve lengths ($a_1 = 1.08\,\text{mm},\ a_2 = b_1 = 3.5\,\text{mm},\ \epsilon_{rI} = 2,\ a_3 = 4.5\,\text{mm},\ d_2 = d_1 = d_0 + h,\ d_3 = d_2 + l + s$).

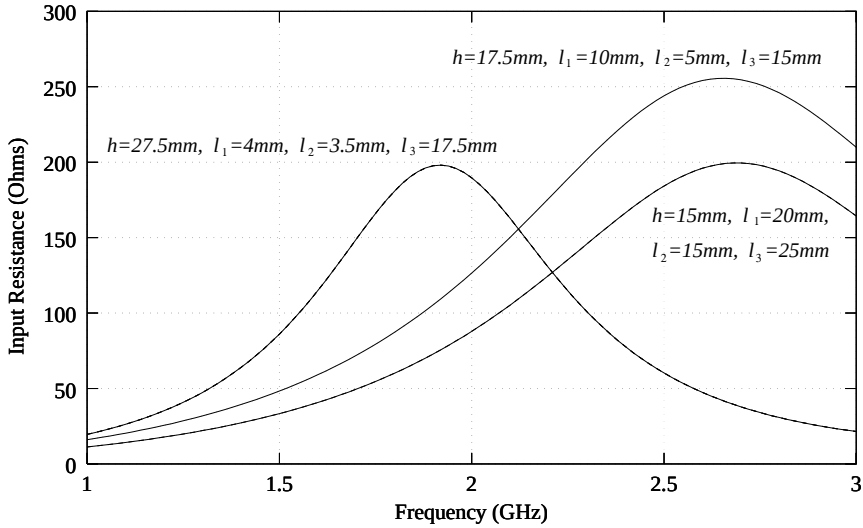

(a) Input resistance

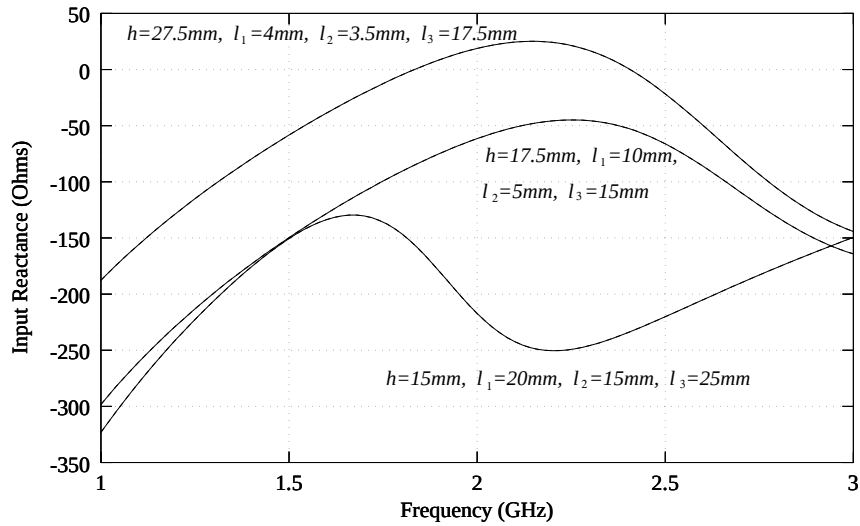

(b) Input reactance

Figure 9. Input impedance of double-sleeve monopole antennas with different monopole and sleeve lengths ($a_1 = 1\,\text{mm}, a_2 = b_1 = 4\,\text{mm}$, $\epsilon_{rI} = 1$, $a_3 = 4.25\,\text{mm}$, $a_4 = 5.25\,\text{mm}$, $a_5 = 5.5\,\text{mm}$, $d_2 = d_1 = d_0 + h$, $d_3 = d_2 + l_1$, $d_4 = d_3 - l_2$, $d_5 = d_4 + l_3 + s$).

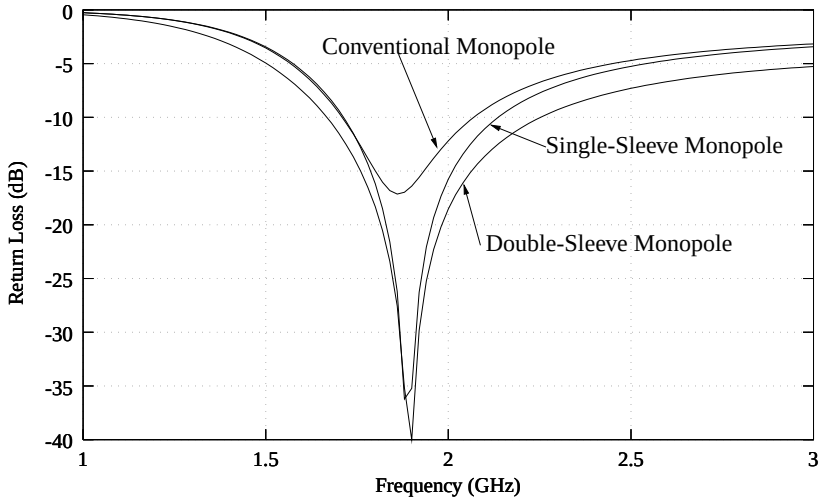

Figure 10. Comparison of the return loss of conventional monopole, single-sleeve monopole, and double-sleeve monopole antennas (Parameters are given in Figs. 5, 6, 7, respectively).

tional monopole. The double-sleeve monopole antenna exhibits even wider bandwidth than single-sleeve monopole. The -10 dB return loss bandwidth of the double-sleeve monopole is 30%, and the -20 dB return loss bandwidth is 8.8% without any impedance matching structure. This is certainly a remarkable advantage of using double-sleeve monopole antenna since the minimum return loss of the conventional monopole antenna is about -17 dB, as seen in Fig. 10.

Figures 11 and 12 shows the current distribution and radiation pattern of a conventional monopole. It is seen that the current is almost zero at the end of the monopole and the current distribution variation depends on the electrical length $(d_1 - d_0)/\lambda$ of the monopole. Figures 13 and 14 presents the current distribution and radiated field pattern of a single-sleeve monopole. Similar to the observations on the input impedance, the current distribution changes quite a lot for different values of monopole length and sleeve length. Radiation patterns also differ from each other, though in a much insignificant way. Figures 15 and 16 gives the current distribution and radiation pattern of a double-sleeve monopole antenna. Since the current on the monopole and sleeve surfaces very well approximates the quasi-sinusoidal variation, the radiation pattern is very much similar to that of a quarter-wavelength monopole, as noted in in Fig. 16.

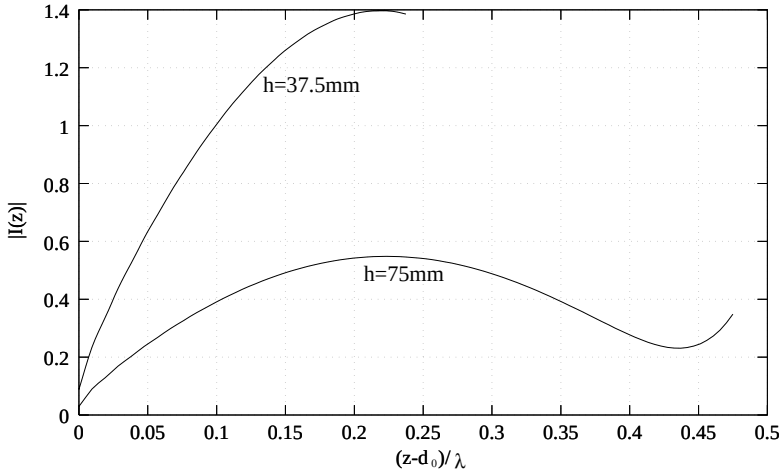

Figure 11. Current distribution on conventional monopole antennas ($a_1 = 1.08\,\text{mm},\ a_2 = b_1 = 3.5\,\text{mm},\ \epsilon_{rI} = 2,\ f = 1.9\,\text{GHz}$) .

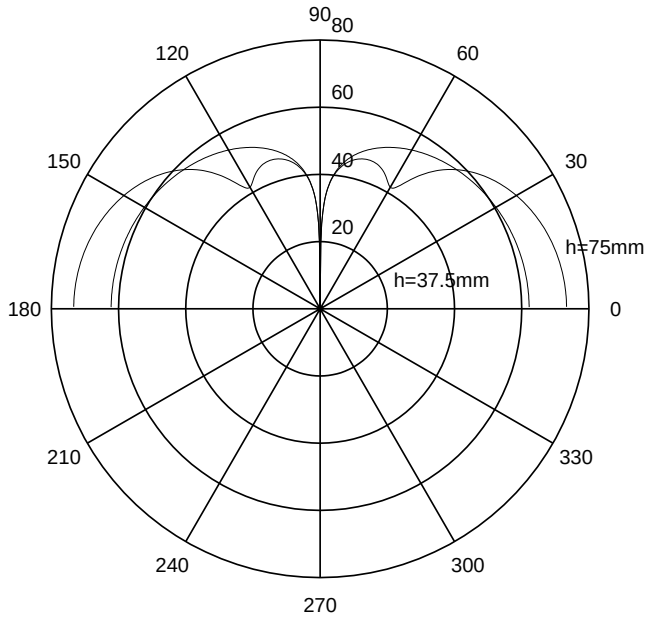

Figure 12. Radiation pattern of conventional monopole antennas (Same parameters as in Fig. 11).

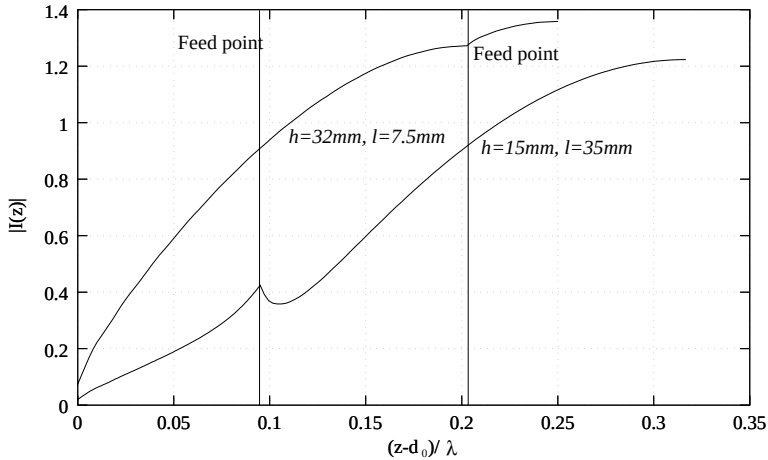

Figure 13. Current distribution on single-sleeve monopole antennas ($a_1 = 1.08\,\text{mm},\ a_2 = b_1 = 3.5\,\text{mm},\ \epsilon_{rI} = 2,\ a_3 = 4.5\,\text{mm},\ d_2 = d_1 = d_0 + h,\ d_3 = d_2 + l,\ f = 1.9\,\text{GHz}$).

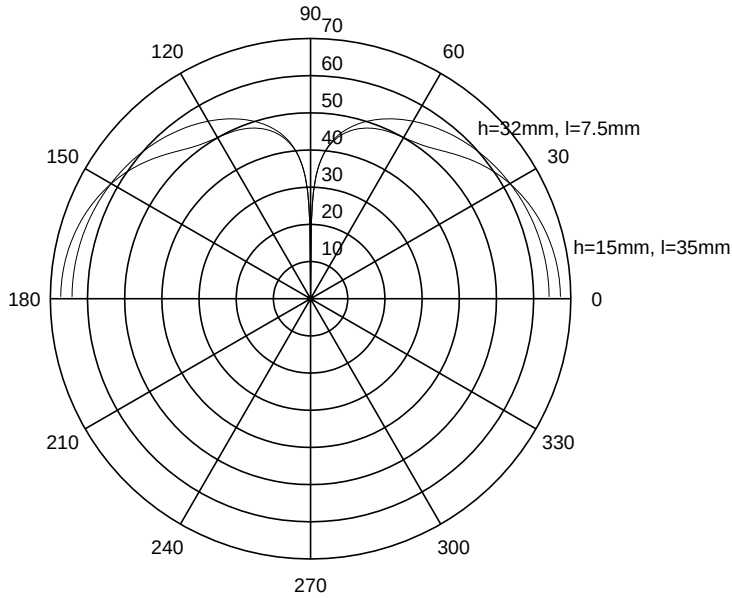

Figure 14. Radiation pattern of single-sleeve monopole antennas (Same parameters as in Fig. 13.)

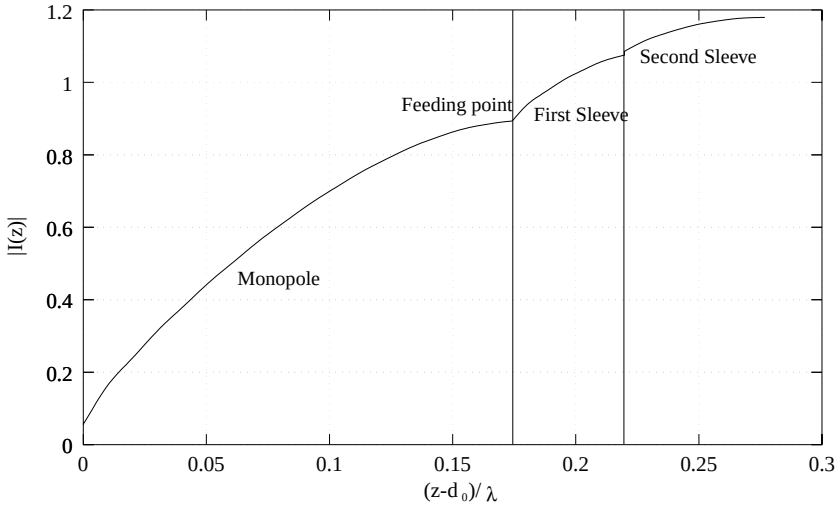

Figure 15. Current distribution on a double-sleeve monopole antenna ($a_1 = 1\,\text{mm},\ a_2 = b_1 = 4\,\text{mm},\ \epsilon_{rI} = 1,\ a_3 = 4.25\,\text{mm},\ a_4 = 5.25\,\text{mm},\ a_5 = 5.5\,\text{mm},\ d_1 = d_2 = d_0 + 27.5\,\text{mm},\ d_3 = d_2 + 11.2\,\text{mm},\ d_4 = d_2 + 4\,\text{mm},\ d_5 = d_2 + 9\,\text{mm} + s$).

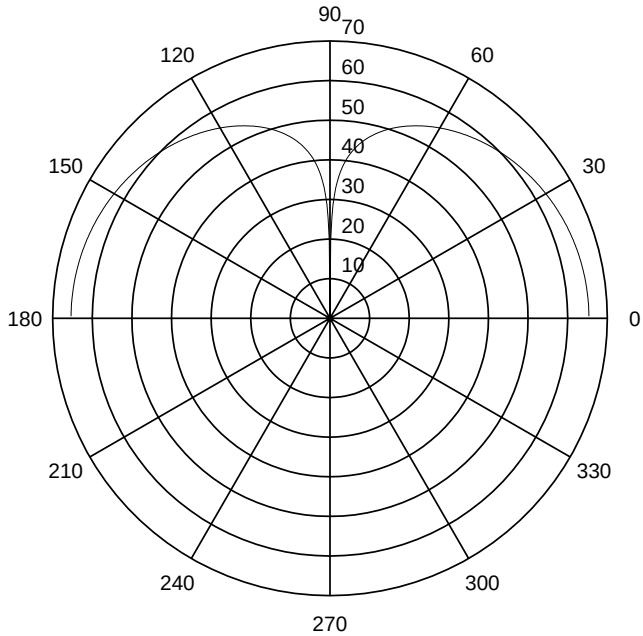

Figure 16. Radiation pattern of a double-sleeve monopole antenna (Same parameters as in Fig. 15).

4. CONCLUSIONS

This paper has provided a rigorous modal-expansion analysis of the current distribution and input admittance of a multi-sleeve monopole antenna driven through an infinite conducting ground plane from a coaxial line. The presented method has no limitation on the radii of the monopole and the sleeves and is applicable to a monopole antenna with arbitrary number of sleeves.

Extensive computed results have been presented for the current distributions, input impedances, and radiation patterns of single- and double-sleeve monopole antennas. The bandwidth of a double-sleeve monopole antenna has been studied in detail and compared to that of the conventional monopole and a single sleeve monopole.

ACKNOWLEDGMENT

One of the authors (Z. Shen) would like to acknowledge a Postdoctoral Fellowship from Natural Sciences and Engineering Research Council (NSERC) of Canada. He is also very grateful to Professors R. W. P. King and T. T. Wu of Gordon McKay Laboratory, Harvard University for the support and encouragement he received while his stay.

REFERENCES

1. King, R. W. P., *The Theory of Linear Antennas*, Harvard University Press, Cambridge, Mass., 1956.
2. King, R. W. P., *Tables of Antenna Characteristics,* IFI, Plenum, New York, 1971.
3. Taylor, J., "The sleeve antenna," Doctoral Dissertation. Cruft Lab., Harvard Univ., Cambridge, MA, 1950.
4. Poggio, A. J. and P. E. Mayes, "Pattern bandwidth optimization of the sleeve monopole antenna," *IEEE Trans. Antennas Propagat.,* Vol. AP-14, 643–645, Sept. 1966.
5. Rispin, L. W. and D. C. Chang, "Wire and loop antennas," *Antenna Handbook,* Y. T. Lo and S. W. Lee (Eds.), 7.23–7.36, Van Nostrand Reinhold, New York, 1988.
6. Wunsch, A. D., "Fourier series treatment of the sleeve monopole antenna," *IEE Proc. -H,* Vol. 135, No. 4, 217–225, 1988.
7. Shen, Z. and R. H. MacPhie, "Modal expansion analysis of monopole antennas driven from a coaxial line," *Radio Science,* Vol. 31, No. 5, 1037–1046, 1996.
8. Shen, Z. and R. H. MacPhie, "Rigorous evaluation of the input

impedance of a sleeve monopole by modal expansion method," *IEEE Trans. Antennas Propagat.,* Vol. AP-44, No. 12, 1584–1591, 1996.

9. Marcuwitz, N., *Waveguide Handbook*, McGraw-Hill, New York, 1951.
10. Kuhn, E., "A mode-matching method for solving field problems in waveguide and resonator circuits," *Arch. Elek. Ubertragung.,* Vol. 27, 511–518, Dec. 1973.
11. Abramowitz, M. and I. A. Stegun, *Handbook of Mathematical Functions,* Dover, New York, 1965.
12. Morgan, M. A. and F. K. Schwering, "Eigenmode analysis of dielectric loaded top-hat monopole antennas," *IEEE Trans. Antennas Propagat.,* Vol. AP-42, No. 1, 54–63, 1994.
13. Balanis, C. A., *Antenna Theory Analysis and Design,* Harper & Row, New York, 1982.
14. Mittra, R. and S. W. Lee, *Analytical Techniques in the Theory of Guided Waves*, Macmillan, New York, 1971.